NIH Public Access
Author Manuscript
Biochemistry. Author manuscript; available in PMC 2011 August 31.

Published in final edited form as:
Biochemistry. 2010 August 31; 49(34): 7393–7402. doi:10.1021/bi100643y.

Mutation at a Strictly-Conserved, Active-Site Tyrosine in the Copper Amine Oxidase Leads to Uncontrolled Oxygenase Activity†

Zhi-wei Chen[*], **Saumen Datta**[*,#], **Jennifer L. DuBois**[‡,§], **Judith P. Klinman**[‡,¶], and **F. Scott Mathews**[*,¶]

[*]Department of Biochemistry and Molecular Biophysics, Washington University School of Medicine, 660 S. Euclid Avenue, Box 8231, St. Louis, MO 63110.

[‡] Department of Chemistry and Department of Molecular and Cell Biology, University of California at Berkeley, Berkeley, CA 94720.

Abstract

The copper amine oxidases carry out two copper-dependent processes: production of their own redox-active cofactor (2,4,5-trihydroxyphenylalanine quinone, TPQ), and the subsequent oxidative deamination of substrate amines. Because the same active-site pocket must facilitate both reactions, individual active-site residues may serve multiple roles. We have examined the roles of a strictly-conserved active-site tyrosine Y305 in the copper amine oxidase from *Hansenula polymorpha* kinetically, spetroscopically, and, in the present work, structurally. While the Y305A enzyme is almost identical to the wild-type, a novel, highly oxygenated species replaces TPQ in the Y305F active sites. This new structure not only provides the first direct detection of peroxy-intermediates in cofactor biogenesis, but also indicates the critical control of oxidation chemistry that can be conferred by a single active-site residue.

Copper amine oxidases (CAO) comprise a family of enzymes that are found almost ubiquitously among aerobic prokaryotic and eukaryotic organisms. These enzymes catalyze the oxidation of primary amines to aldehydes and reduction of dioxygen to hydrogen peroxide via a ping-pong mechanism involving a covalently-bound redox cofactor, 2,4,5-trihydroxyphenylalanine quinone (TPQ) and a copper ion, Cu(II) (1,2). In conjunction with the multiple catalytic turnovers catalyzed by the mature CAOs, these enzymes catalyze a second, single turnover reaction. The latter process involves the reaction of an active-site tyrosine and molecular oxygen, in a copper-dependent manner, to generate the TPQ cofactor, Scheme 1 (3-5). The active-site Tyr that leads to TPQ (position 405 in the CAO from *Hansenula polymorpha*) is absolutely conserved among CAO family members and is contained within the consensus sequence Thr-X-X-Asn-Tyr-Asp/Glu (4). Other strictly-conserved residues include three histidine residues (His456, His458 and His624) that form

†This work was supported by grants from the National Institutes of Health: GM31611 to FSM, GM039296 to JPK, and GM63414-01 to J.L.D. Use of the Advanced Photon Source supported by the U.S. DOE, Office of Basic Energy Sciences, Contract No. W-31-109-ENG-38.

¶ To whom correspondence should be addressed: JPK: Phone: (510) 642-2668; Fax: (510) 643-6232; klinman@berkeley.edu; FSM: Phone: (314) 362-1080; Fax: (314) 362-7183; mathews@biochem.wustl.edu..
[#]Present address: Structural Biology and Bioinformatics Division, Indian Institute of Chemical Biology, Kolkata-32, PIN-700032, INDIA.
[§]Present address: Department of Chemistry and Biochemistry, University of Notre Dame, Notre Dame, IN 46556.

Supporting Information
This includes occupancies and temperature factors of the final model (**Table S1**), and interactions and associated water molecules in the final model (**Table S2**). This material is available free of charge via the Internet at http://pubs.acs.org.

NIH-PA Author Manuscript
NIH-PA Author Manuscript
NIH-PA Author Manuscript

NIH-PA Author Manuscript

NIH-PA Author Manuscript

NIH-PA Author Manuscript

the three protein ligands to the copper ion and a second Tyr (position 305 in *H. polymorpha*) that is located at the active site near the O-4 position of the TPQ cofactor (Figure 1 A) (6).

There are a number of possible roles that can be considered for Y305 in the course of both catalytic turnover and cofactor biogenesis. For amine oxidation, the close proximity of Tyr 305 to the O-4 of the TPQ anion (Figure 1A) suggests a short, strong hydrogen bond that may be expected to play a role in charge localization and stabilization. The latter are expected to facilitate the formation of a positively charged substrate Schiff base intermediate at the C-5 position of cofactor during the reductive half-reaction. The presence of Tyr 305 has also been proposed to assist in the shuttling of the protons needed for hydrogen peroxide formation from the site of amine oxidation to that of oxygen reduction (7,8). One important feature during catalytic turnover is the requirement for TPQ to be maintained in a fixed conformation. This prevents cofactor from binding to the active-site copper and keeps it near the active-site base (Asp 319) that catalyzes substrate deprotonation/oxidation. Mutation of either the active-site base or other residues within the consensus sequence has been demonstrated to impair catalysis via the formation of non-productive conformations of the cofactor (9,10,11).

In the case of cofactor biogenesis, a number of alternate roles for Tyr 305 have been suggested. These include participation as a general base or acid during oxygenation of the precursor tyrosine side chain, together with a steric role in positioning the Tyr and its oxygenated intermediates that form in route to TPQ (7,8,12,13). One very interesting and mechanistically challenging distinction between cofactor biogenesis and catalytic turnover is the need to access a range of side chain conformations in the course of TPQ production versus the need to keep the cofactor rigid during catalytic turnover.

The role of residue Y305 in amine oxidation and cofactor biogenesis in HPAO has been evaluated through site-directed mutagenesis (7,8). The tyrosine side chain at this position has been replaced with Ala and Phe and the kinetic, spectroscopic and biochemical properties of the mutants measured. In studies of amine oxidation, it was found that Y305A reacted with ethylamine at a rate ~3-fold lower than WT, while the rate for Y305F mutant was reduced more than 100-fold, Table 1 (7). These results were surprising since the Y305F mutation was initially considered to be a more conservative mutation than the Y305A. In subsequent studies of TPQ biogenesis, the Y305F mutant showed rates for cofactor production that were close to that of the wild-type protein (reduced ~3-fold), while the Y305A mutant was significantly more hindered, with a rate of ca. 50-fold slower than Y305F, Table 1 (8). Furthermore, an additional product was formed in the two mutants that increased with pH and, significantly, lacked the spectral properties expected for a precursor-product relationship with regard to the TPQ (8). This has implicated two parallel pathways during cofactor biogenesis in the case of Tyr 305 mutants, with one pathway leading to the expected TPQ product while the other produces a new, unknown species.

In this paper, we present X-ray structures for the Y305 mutant that either preserves catalytic activity during turnover, Y305A, or maintains high rates for cofactor biogenesis, Y305F. Two key results from the studies presented herein are (i) the demonstration that the structure for Y305A is almost identical to wild-type enzyme, and (ii) the detection of a new multiple peroxo- species in the course of TPQ biogenesis with Y305F. The latter points toward an uncontrolled oxidative process that takes place upon deletion of a hydroxyl group from Y305A, with the aggregate data providing a rationale for the absolute conservation of this side chain among all known copper amine oxidases.

NIH-PA Author Manuscript

NIH-PA Author Manuscript

NIH-PA Author Manuscript

Materials and Methods

Crystal Structure Determination

Mature Y305A and Y305F were expressed as the holoproteins in *S. cerevisiae* and purified as described previously (7). The enzymes were stored at 12.3 mg/mL and 25.1 mg/mL, respectively, in 50 mM KPi buffer, pH 7.2. Apo-Y305F was expressed in *E. coli* and reconstituted with Cu(II) at pH 6.5 as described previously (8). The reconstituted enzyme was exchanged into neutral buffer (50 mM HEPES, pH 7.0) and concentrated to 10 mg/mL. For each protein sample, crystal growth was carried out using the hanging drop-vapor diffusion procedure (14) by mixing 2.5 μL protein solution with an equal amount of precipitant solution and equilibrating the mixture at room temperature against the precipitant solution through vapor interchange for several days. For Y305A, the precipitant was 10% PEG8000 and 125 mM lithium sulfate in 100 mM KPi buffer, pH 6.3. For yeast-expressed Y305F, the precipitant was 8% PEG8000 in 200 mM KPi buffer, pH 6.4; for the *E. coli*-expressed Y305F, the precipitant was 20% PEG8000, 100 mM HEPES, pH 7.5 and 2% ethylene glycol.

Data from all crystals were collected at the Advanced Photon Source, Argonne, IL. For Y305A and yeast-expressed Y305F, the data were recorded to 2.50 Å and 1.90 Å resolution, respectively, on a 3 × 3 CCD detector at beamline 19ID of the Structural Biology Center; for the *E. coli*-expressed Y305F mutant a Quantum IV CCD detector to collect data to 2.05 Å resolution was used at beamline 14BMC of BIOCARS. In all cases, the crystals were flash-frozen at 100K prior to data collection after treatment with mother liquor containing 25% glycerol for the yeast-expressed mutants and 15% glycerol for the *E. coli*-expressed mutant for 3-4 minutes. The data were indexed, integrated and scaled using HKL2000 (15).

All three structures were solved by molecular replacement, using AMORE (16) for the yeast-expressed mutants and MOLREP (17) for the *E. coli*-expressed mutant. Subunit 1 of the native HPAO structure (PDB code 1A2V) was used as the search molecule for each. In all cases, the side chains of Y305, TPQ405 and all water molecules were omitted from the search model. Each structure was then refined using CNS (18); water molecules were gradually added using the water-searching procedure. When no more waters could be added, difference maps were calculated to identify and model residue 305. Alanine could clearly be modeled into the Y305A structure and phenylalanine into both Y305F structures. In the later stages of refinement, strict NCS (non-crystallographic symmetry) constraints were used. Simulated annealing omit maps were then calculated using CNS (18) by omitting all residues containing atoms within 3.5 Å of residue 405; they were then 6-fold averaged on the basis of the strict NCS refinement matrices.

For the Y305A mutant, TPQ could clearly be modeled into the omit map density and corresponded closely in position and orientation to that of the native structure. Subsequent refinement in CNS yielded (2Fo-Fc) and (Fo-Fc) maps that were consistent with the fit to the omit map. For the Y305F mutants, the electron density was fit with a derivative of the wild-type tyrosine side chain that was consistent with the omit map density, as described in **Results**.

Structural diagrams

Structural diagrams were rendered using PYMOL (available on the World Wide Web at www.pymol.org).

NIH-PA Author Manuscript

NIH-PA Author Manuscript

NIH-PA Author Manuscript

Results

Crystal Structure Analysis

Efforts to obtain the structure of the new product arising during the biogenesis of the Y305 variants of the *H. polymorpha* copper amine oxidase initially involved mass spectrometry. However, in all efforts made so far, a broad envelope of masses was observed, presumably due to the heterogeneity of the protein samples and the breakdown of the protein modification during analysis. For this reason, we turned to X-ray crystallography as the primary means of structure determination. Crystals of both Y305A and Y305F were obtained for protein expressed in *S. cerevisiae* (7,19) whereas enzyme expressed as the apoenzyme in *E. coli*, reconstituted with Cu(II) under anaerobic conditions at pH 6.5 and then exposed to air (8,20) produced crystals only of the Y305F mutant. The space group symmetry information and unit cell parameters of the three crystals are given in Table 2. All three crystals contained six identical protomers (three dimeric HPAO molecules) in the asymmetric unit. After preliminary tests using non-crystallographic symmetry restraints, each of the three structures was refined in CNS (18) using strict non-crystallographic symmetry (NCS) constraints during the final stages, thereby reducing by 6-fold the number of refinement variables. This procedure partially offset the relatively limited completeness of the three data sets at the highest resolution (Table 2), resulting from loss of data that occurred from excessive overlap of reflections caused by the relatively long unit cell edges and the high mosaic spread of the reflections from the crystals. The advantageous use of strict NCS for improving the accuracy of the structure is reflected by the small spread of R_{cryst} and R_{free} in the final refinement parameters (Table 2). The final models for the two yeast-expressed mutants contain 655 residues and for the *E. coli* mutant, 661 residues; the Y305A mutant contains one modified amino acid side chain (Tyr405) compared to two modified amino acid side chains (Tyr405 and Met634, see below) for the two Y305F mutant structures. The number of solvent molecules and extraneous chemical species identified in each structure, as well as an analysis of the stereochemistry of each of the three structures using PROCHECK (21), are presented in Table 2.

Structure of Y305A

The structure of the Y305A mutant of HPAO is very similar to that of the wild-type enzyme. When the strict symmetry-constrained mutant structure is compared with subunit A of the wild-type enzyme, the rmsd for all 655 matched C-atoms is 0.21 Å. The active site of the Y305A mutant is shown in Figure 2. Its configuration is the catalytically active one since atom O5 of TPQ is oriented near Asp319 (the catalytic base), is accessible to the substrate entry channel and is available for binding to the amine substrate. Also included in Figure 2 are eight water molecules located in the active site of Y305A that are all present in the native structure, including one that bridges atom O2 of TPQ to the copper ion.

Structure of Y305F

The 6-fold averaged simulated annealing omit maps of both Y305F mutant crystals were initially difficult to interpret in the region of the active site near the expected TPQ binding site. The omit map for the *E. coli*-expressed mutant was minimally consistent with TPQ in a copper on orientation, with O5 coordinated to the copper ion at a distance of 3.0 Å (Figure 3A). However, additional electron density protruded from the O4 position, the density near O2 was weak and a peak at the 3-sigma contour level that connected to the ring at the 2.5 sigma level was present near C3. A better fit to this density could be achieved with an additional oxygen atom, O4A, attached to O4 and atom O2 eliminated (Figure 3B), creating a peroxo- derivative of Tyr405 initially referred to as the parent TPO structure (TPO-4). Difference maps computed using (2Fo-Fc) and (Fo-Fc) coefficients from either of these models gave indications there might be a mixture of TPO and TPQ present and that residual

NIH-PA Author Manuscript

NIH-PA Author Manuscript

NIH-PA Author Manuscript

water molecules might also be present close to the cofactor ring; however, additional refinements and map calculations were unsatisfactory. Closer examination of these difference maps and of the original simulated annealing omit map suggested strongly that, instead, the maps could be best fit with peroxo- groups at C2 and C3, in addition to C4, as well as the oxygen at C5 (Figure 3C). This interpretation was corroborated by comparison of a model with multiple peroxo- groups to the simulated annealing omit map obtained with the yeast-expressed Y305F mutant (Figure 3D). Refinement of the model using X-ray data from either the yeast or *E. coli*-derived Y305F at full occupancy yielded (Fo-Fc) electron density difference maps with negative peaks near the O2, O2A and O3, O3A positions of up to 4.5 to 5.0 sigma in magnitude which, when considered with their relatively weak density in the omit map suggested that these sites are only partially occupied. Refinement with these four sites at 50% occupancy in both crystals yielded (Fo-Fc) difference maps showing no difference electron density of magnitude 3 sigma or greater at these sites, indicating that the 50% occupancy level was approximately correct. There was, however, some negative difference density close to the O4 position in both crystals of magnitude ~3.5-4 sigma, suggesting that the O4 atom was undergoing considerable thermal motion, as reflected in the refined B-factors (Table S1).

In the process of monitoring the peroxo-oxygen occupancies by computing (Fo-Fc) difference maps for the two Y305F mutant crystals, a persistent positive difference density peak of magnitude 3.5-4 sigma was found close to the $C^{EPSILON}$ atom of Met634, a feature also visible in the omit maps (Figures 3C and 3D). These features suggested that a nascent oxygen atom had become attached to the methyl group of Met 634 during the oxygenation of residue 405. To test this possibility, further refinement using CNS was carried out in which an oxygen atom, O^{ZETA}, was bound to Met634 at 50% occupancy. Subsequent difference maps supported the assignment of this modification of the M634 side chain.

The final model for the Y305F mutants of HPAO expressed in both *S. cerevisiae* and *E. coli* contains a side chain at position 405 consisting of a phenyl ring with a peroxo group attached at C4 and an oxygen atom bound at position C5, both at full occupancy (TPO), and with peroxo- groups at positions C2 (TPO-2,4) and C3 (TPO-3, 4) at approximately half occupancy. In addition, a modified Met634 side chain containing an additional oxygen atom, O^{ZETA}, at half occupancy is present. Also included are three waters (W1-W3), that form a hydrogen bonding cluster with atoms O2, O2A and O3A of TPO and two side chains, and a fourth water (W4) that interacts with atom O4A and a nearby carbonyl. The final active-site electron density difference maps are given in stereo in Figure 4 and a model indicating hydrogen-bonding interactions is given in Figure 5. The hydrogen-bonding distances for the interactions of Figure 5 are summarized in Table S2.

Discussion

Structural Analysis of the Y305F Mutant

When the simulated annealing omit maps of the yeast- and *E. coli*-expressed Y305F mutants were first examined, it was evident that the structure of the active form of HPAO (as shown in Figures 1A and 2), with the O5 of TPQ oriented in the direction of the active-site base, Asp319 and O2 linked to the copper ion via a bridging water molecule, could not represent the true configuration of residue 405. Nor were the omit maps consistent with the presence of a modified tyrosine side chain bound to copper through the O4 position similar to the position of the unmodified tyrosine in the structure of the zinc-substituted enzyme (as shown in Figure 1B). Rather, there appeared to be a mixture of species present.

One distinctive feature of the *E. coli* map was a strong peak close to O4 of the putative cofactor, too close to be a hydrogen-bonded water, but suggestive of a peroxo- intermediate.

NIH-PA Author Manuscript

NIH-PA Author Manuscript

NIH-PA Author Manuscript

This feature was also present in the map of the yeast-expressed mutant, although prominent additional unexplained density was present at positions 2 and 3 of the ring. To eliminate the possibility that these peaks were caused by radiation damage during exposure of the crystals to the X-ray beam at the synchrotron, each data collection run was divided into three sequential “time slices”, which were analyzed by computing 6-fold averaged simulated annealing omit maps using the NCS matrices derived during structure refinement of the full data sets. Although each “time slice” was only 50 to 60% complete, the 6-fold averaging procedure of the final maps partially compensated for the incompleteness of the data. While some variations were observed among the time slices, there was no correlation between the detection of peroxo- species and the X-ray exposure time.

The relative occupancies of the oxygen atoms that are attached to position 405 have been estimated. The TPQ cofactor and its variant are derived from a gene-encoded tyrosine side chain within the amino acid sequence. Therefore, the occupancy of the tyrosyl portion must be constant, as there is no reasonable chemical mechanism that could result in removal of the O4 oxygen of a tyrosine during cofactor biogenesis. The occupancies of the six-carbon atoms of the ring and of O4 were, thus, maintained with a value of 1.0. The simulated annealing omit maps of the two crystals also indicate strong density for the O5 oxygen that is coordinated to the copper ion suggesting full occupancy. In a test refinement with each of the two crystals in which the occupancy of the O5 atom of the model was assigned the value of 0.5, the resulting (Fo-Fc) difference map contained positive difference density peaks at the 4-sigma level at the O5 position, confirming the site is fully occupied. This is also consistent with the chemistry since a 6-membered ring lacking the O5 atom would be unlikely to maintain its position so close to the copper without a coordination bond.

On the other hand, the peroxo- substitutions at the C2 and C3 positions do not appear to be fully occupied. In the omit map of the *E. coli*-expressed mutant (Figure 3C) the 3-sigma contour surface lies close to the C2 and C3 atoms of the ring, although there is a 3-sigma peak close to atom O3A. However, the 2.5-sigma contour surface does envelop all four atoms nearly completely. In the omit map of the yeast-expressed mutant (Figure 3D) the 3-sigma contour surface envelopes the O3 and O3A atoms and nearly envelopes the O2 atom while the 2.5 sigma contour fully envelopes all four atoms. The relative occupancies of the C2 and C3 oxygens appear to be greater for the yeast-expressed than for the *E. coli*-expressed mutants, especially when the final (2Fo-Fc) maps are compared (Figures 4A and 4B). However, for both mutant crystals the substitution at C3 appears to be stronger than for C2.

A semi-quantitative estimate of the occupancies of the C2 and C3 peroxo atoms was also obtained by refining the final TPO model with various occupancies imposed on the atoms. When all four atoms were assigned zero occupancy the (Fo-Fc) difference maps showed strong positive features close to the atom positions while assignment of full occupancies yielded equally strong negative peaks. Setting their occupancy values to 0.5 reduced the magnitude of the difference density to below the 3-sigma level. An occupancy value of 0.5 was also obtained in this manner for the terminal oxygen, O^{ZETA}, of Met634. The refined temperature factors for the oxygen atoms of TPO405 and the oxygen-substituted Met634 are consistent with their assigned occupancies (Table S1) and correlate reasonably well with their hydrogen bonding environments (Figure 5, Table S2).

Relationship of the Structure of Y305A to Efficiency of Catalytic Turnover

Y305A shows kinetic behavior close to wild-type (Table 1), despite the lack of the short strong hydrogen bond to TPQ O4 seen in the structure for the wild-type enzyme, Figure 1A. One possible explanation offered for the high activity of Y305A was the creation of a cavity for water(s), with the expectation that one of these water molecules would assume the role

NIH-PA Author Manuscript

NIH-PA Author Manuscript

NIH-PA Author Manuscript

of a hydrogen-binding entity (7,22). It is, therefore, somewhat surprising that the structure for Y305A is virtually identical to that for wild-type, with the exception of the absence of the Tyr side chain at position 305. Although water cannot be visualized in the cavity created by the deletion of Y305, it is possible that waters are present but simply too disordered to be observed in the 2.5 Å resolution X-ray structure.

A second possibility is that the hydrogen-bonding functionality of Tyr305 is simply not essential for catalysis and that the primary role for Y305 is in the biogenesis pathway (see below). The explanation for the low activity with Y305F is the introduction of a hydrophobic residue near the anionic TPQ, which leads to destabilization and rotation of the TPQ into a non-productive conformation. In the previously determined structure of the analogous Tyr to Phe mutant in the *E. coli* CAO, the presence of Phe was shown to lead to rotation of the TPQ into a non-catalytic position where it underwent hydrogen bonding with a copper-bound water molecule (13). The similarity between the kinetic and structural data for Y305A and wild-type enzyme rules out an essential role for a short, strong H-bond from Tyr 305 TPQ during amine oxidation or O_2 reduction. Further, the structural data for Y305A indicate that conserved residues other than Y305 must assume the role of anchoring the TPQ into its correct, catalytically relevant conformation within the active site of HPAO (cf. 23).

Relationship of the Structure of Y305F to the Mechanism for Cofactor Biogenesis

The mechanism for cofactor biogenesis has been studied by a variety of kinetic, spectroscopic and structural approaches, leading to the working mechanism in Scheme 1 (cf. 24,25). As illustrated, binding of O_2 to the Cu(II)-reconstituted enzyme is a “trigger” for the movement of the TPQ precursor (Tyr 405 in HPAO) onto the active-site metal. Support for a “metal-on” structure during biogenesis in HPAO has come from the X-ray structure for the Zn^{+2}-reconstituted enzyme, illustrated in Figure 1B (25). While zinc ion binds tightly to HPAO in a competitive manner with copper ion, it is unable to support the subsequent oxygenation of the tyrosine ring. Spectroscopic and time-resolved X-ray studies implicate a central role for a charge transfer band between the tyrosine precursor and copper ion, leading to a mechanism in which the metal activates the substrate (Tyr 405) for reaction with O_2 (23,24). The resulting chemical intermediate, the peroxo- derivative of tyrosine formed by addition of O_2 to the activated Tyr ring, has never been observed, though it is considered a key feature of the postulated mechanism. Breakdown of this peroxo- intermediate produces a dopaquinone species, which then undergoes a nucleophilic attack by a copper-bound water/hydroxide ion to generate the reduced form of TPQ. One distinctive feature of this mechanism is the need for Tyr 405 and its resulting intermediates to undergo considerable conformational movement involving the formation of both “on-metal” and “off-metal” complexes, as well as rotations about the α-β and β-γ side chain bonds of the Y405 side chain.

The kinetic data for the Y305A and Y305F mutants have revealed an unexpected property, specifically an impact of mutation on biogenesis that is opposite to that seen for catalysis, Table 1. As a first approximation, steric bulk at position 305 emerges as a likely factor, perhaps to guide the Tyr-derived intermediates into one or more of the conformations that must be accessed for successful biogenesis. It is of considerable interest that mutation of Y305 also leads to a faster rate of production of an alternate species, formed in parallel to TPQ for both Y305A and Y305F (8). These features of the biogenesis are summarized in eq (1) for the condition of pH 7 (8):

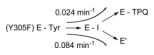

(1a)

NIH-PA Author Manuscript

NIH-PA Author Manuscript

NIH-PA Author Manuscript

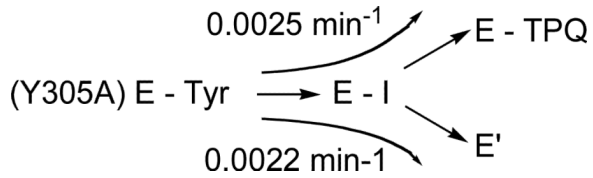

(1b)

The combined kinetic properties for Y305F and Y305A strongly suggest the formation of a common intermediate from which both TPQ and its inactive variant are formed. The structures obtained for Y305F, Figures 3-5, allow us to propose a chemical pathway that will explain the aggregate experimental data.

Accordingly, it is postulated that E-I in eq (1) is the initial peroxy- intermediate formed from the rate-limiting addition of O_2 to the activated, charge-transfer complex between Y405 and the active-site copper. It is likely that the size of the residue at position 305 plays an important role in the rate of formation of the initial charge-transfer complex and/or its conversion to the peroxo- intermediate. Once the peroxo- intermediate is formed, it has two options, which once again, depends on the nature of the side chain at position 305, Scheme 2. In the normal pathway that produces TPQ, we propose that ring rotation places the peroxo- functional group near Y305 such that the hydroxyl group of this tyrosine can facilitate the O-O bond cleavage that is essential for the formation of dopaquinone and copper hydroxide. Model building of the rotated conformation for E-I, using the structure in Figure 1B of the zinc-containing HPAO precursor (24), indicates a distance of ca. 2.5 Å between the Y305 hydroxyl group and O3A in Y405. When Y305 is mutated to the hydrophobic Phe, an alternate pathway is proposed to arise in which ring rotation is inhibited and deprotonation at C5 leads to ring aromatization, rather than O-O bond cleavage. Although an earlier biochemical analysis failed to detect an aryl-peroxide species during biogenesis of Y305A at high pH (8), this is attributed either to an inaccessibility of the reagent to the peroxo- functional group and/or a decomposition of the peroxide under the conditions of the assays. Thus, while Y305F can approximate the wild-type enzyme in the rate-limiting formation of the initial peroxo- intermediate (E-I in Scheme 2A), the Phe at 305 greatly favors the non-productive pathway leading to TPO, explaining our ability to grow crystals of E' in the case of Y305F. The fact that the ratio of TPO to TPQ formation is less for Y305A than Y305F is likely a consequence of the much-reduced hydrophobicity of an Ala side chain, together with a possible access of solvent water, which could aid in the O-O bond cleavage step.

The structures for Y305F presented herein reveal that the aberrant oxidative chemistry seen in Scheme 2A does not stop at TPO formation. The data indicate that further activation of the initially derivatized ring occurs via a coordination to the active site Cu(II). To recapitulate, the chemical composition of the final model of the TPO cofactor is an approximately equimolar mixture of the TPO-3,4 and TPO-2,4 (Scheme 2B) which is represented in the X-ray structure as a phenylalanine side chain substituted by a hydroxyl group and a peroxo group at full occupancy at positions 5 and 4, respectively, and by peroxo groups at approximately half occupancy at positions 3 and 2, respectively. We note that the electron density could also be consistent with an equimolar distribution of TPO-4 and TPO-2,3,4. However, the oxidation mechanism (Scheme 2B) makes it difficult to rationalize how TPO-4, chemically activated for O_2 addition *para*- to the ring hydroxyl, would fail to undergo further reaction. As illustrated in Scheme 2B, mobility of the aromatic ring at position 405, together with an anticipated reactivity of the Cu(II)-phenolate complex at both *ortho*- positions, is proposed to promote the addition of a second molecule of O_2 to yield the

NIH-PA Author Manuscript

NIH-PA Author Manuscript

NIH-PA Author Manuscript

3,4-diperoxo- adduct. Inspection of X-ray structures for Y305F indicates an unexpected property in which a hydroxyl group is on C5 concomitant with the appearance of a hydroperoxide at C4. This necessitates an additional chemical step that involves an intramolecular migration of the terminal hydroxyl group at C5 to the C4 oxygen. Repositioning of the final structure, to optimize coordination to the Cu(II) center, produces TPO-3,4.

In addition to electron density attributed to a hydroperoxide at C3, the electron density maps indicate occupancy by a similar functional peroxo- group at C2, albeit at somewhat reduced occupancy. A mechanism that would produce such a structure is shown in Scheme 2C. In this instance, migration of a hydroxyl group precedes ring rotation, placing the resulting Cu(II)-phenolate complex in a position to activate the ring for further peroxidation at either the *ortho*- or *para*- position. Since the final product shows reaction exclusively at the *para*-position, it is concluded that steric crowding at the site of oxygen reactivity necessitates a ring rotation prior to O_2 insertion. This produces the TPO-2,4, which analogous to TPO-3,4, undergoes a final re-positioning within the pocket to achieve optimal complexation to the copper center. We note the ability of Schemes 2B and C to predict, via a repeating pattern of charge-transfer complex formation proximal to a bound O_2 molecule, the observed atomic occupancies seen in the electron density maps: 100% for O5 and O4, O4A, together with partial occupancies at O3, O3A and O2, O2A.

The superposition of the products formed via Schemes 2B and C generates the final electron density maps observed with Y305F derived from both *E. coli* and *S. cerevisiae* expression, Figures 3 and 4. The slight differences between the *E. coli* and *S. cerevisiae* maps are likely a result of small differences in the partitioning of either TPO or its precursor toward the further oxidation products, TPO-3,4 and 2,4, respectively. In all cases, the same inherent chemical reactivity is at play: formation of a phenolate-Cu(II) charge-transfer complex that activates the aromatic ring at either an *ortho*- or *para*- position for combination with a pre-bound triplet state O_2 molecule. Breakdown of the resulting intermediate via aromatization rather than O-O bond cleavage repeats the pattern of stable peroxo- adduct formation.

One final question that remains to be explained is why the side chain of M634 shows evidence for partial occupancy by a hydroxyl substituent at its methyl group within the O_2-binding pocket. This is postulated to arise via reaction of TPO-2,4 which can orient its C2 peroxo- group in close proximity to the methionine side chain. The transfer of the O2A oxygen, as illustrated below, produces an alcohol rather than peroxo- substituent at C2 together with a hydroxylated methionine. In support of eq (2), careful inspection of the electron density maps of Figures 3 and 4 indicates that the weakest continuous density lies between the O2 and O2A positions:

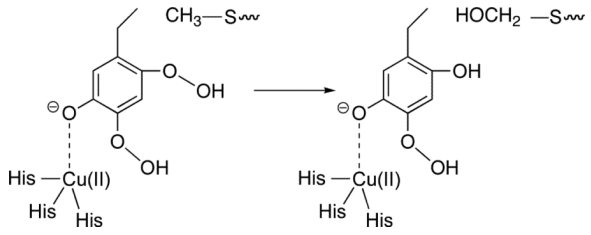

(2)

NIH-PA Author Manuscript

NIH-PA Author Manuscript

NIH-PA Author Manuscript

Conclusion

This work presents, for the first time, X-ray structures for peroxo- intermediates formed during the biogenesis of TPQ from its Tyr precursor. The mutation of Y305F is proposed to interfere with the normal O-O bond cleavage essential to dopaquinone and TPQ formation. Once the first "off-path" intermediate has formed, the inherent properties of the active site – the formation of a Cu(II)-phenolate complex adjacent to an O_2-binding pocket – promote further O_2 addition at activated ring positions. From an evolutionary perspective, the introduction of a hydroxyl group into the phenylalanine ring appears to have been sufficient to suppress an "explosion" of active-site oxygen chemistry, permitting the formation of a biochemically viable cofactor structure. These findings may be highly relevant to non-specific oxidative damage of tyrosine side chains in proteins and peptides that could arise via the adventitious binding of copper ions to form phenolate-copper charge transfer complexes.

Supplementary Material

Refer to Web version on PubMed Central for supplementary material.

Acknowledgments

We thank Dr. Stephen Mills (currently a Professor at San Diego University) for the preparation of the Y305A and Prof. Carrie Wilmot (University of Minnesota) for critical reading and invaluable comments on an earlier draft. We thank the staff at the SBC and BIOCARS of the Advanced Photon Source for assistance and use of equipment.

Abbreviations

CAO	copper amine oxidase
TPQ	2,4,5-trihydroxyphenylalanine quinone
HPAO	copper amine oxidase from *Hansenula polymorpha*
TPO	a generic term indicating one or more peroxo- group on the Y405 ring

References

1. Klinman JP, Mu D. Quinoenzymes in biology. Annu. Rev. Biochem. 1994; 63:299–344. [PubMed: 7979241]
2. Hartmann C, Dooley DM. Detection of reaction intermediates in topa quinone enzymes. Methods Enzymol. 1995; 258:69–90. [PubMed: 8524165]
3. Janes SM, Mu D, Wemmer D, Smith AJ, Kaur S, Maltby D, Burlingame AL, Klinman JP. A new redox cofactor in eukaryotic enzymes: 6-hydroxydopa at the active site of bovine serum amine oxidase. Science. 1990; 248:981–987. [PubMed: 2111581]
4. Mu D, Janes SM, Smith AJ, Brown DE, Dooley DM, Klinman JP. Tyrosine codon corresponds to topa quinone at the active site of copper amine oxidases. J. Biol. Chem. 1992; 267:7979–7982. [PubMed: 1569055]
5. Cai D, Klinman JP. Evidence for a self-catalytic mechanism of 2,4,5-trihydroxyphenylalanine quinone biogenesis in yeast copper amine oxidase. J. Biol. Chem. 1994; 269:32039–32042. [PubMed: 7798196]
6. Li R, Klinman JP, Mathews FS. Crystal structure of copper amine oxidase from *Hansenula polymorpha* determined at 2.4 Å resolution. Structure. 1998; 6:293–307. [PubMed: 9551552]
7. Hevel JM, Mills SA, Klinman JP. Mutation of a strictly conserved, active-site residues alters substrate specificity and cofactor biogenesis in a copper amine oxidase. Biochemistry. 1999; 38:3683–3693. [PubMed: 10090756]

NIH-PA Author Manuscript NIH-PA Author Manuscript NIH-PA Author Manuscript

8. DuBois JL, Klinman JP. Role of a strictly conserved active site tyrosine in cofactor genesis in the copper amine oxidase from *Hansenula polymorpha*. Biochemistry. 2006; 45:3178–88. [PubMed: 16519513]

9. Cai D, Dove J, Nakamura N, Sanders-Loehr J, Klinman JP. Mechanism-based inactivation of a yeast methylamine oxidase mutant: implications for the functional role of the consensus sequence surrounding topaquinone. Biochemistry. 1997; 36:11472–11478. [PubMed: 9298967]

10. Plastino J, Green EL, Sanders-Loehr J, Klinman JP. An unexpected role for the active site base in cofactor orientation and flexibility in the copper amine oxidase from *Hansenula polymorpha*. Biochemistry. 1999; 38:8204–8216. [PubMed: 10387066]

11. Murray JM, Saysell CG, Wilmot CM, Tambyrajah WS, Jaeger J, Knowles PF, Phillips SEV, McPherson MJ. The active site base controls cofactor reactivity in *Escherichia coli* amine oxidase: X-ray crystallographic studies with mutational variants. Biochemistry. 1999; 38:8217–8227. [PubMed: 10387067]

12. Mure M, Kurtis CR, Brown DE, Rogers MS, Tambyrajah WS, Saysell C, Wilmot CM, Phillips SEV, Knowles PF, Dooley DM, McPherson MJ. Active site rearrangement of the 2-hydrazinopyridine adduct in *Escherichia coli* amine oxidase to an azo copper(II) chelate form: a key role for tyrosine 369 in controlling the mobility of the TPQ–2HP adduct. Biochemistry. 2005; 44:1583–1594. (2005). [PubMed: 15683242]

13. Murray JM, Kurtis CR, Tambyrajah W, Saysell CG, Wilmot CM, Parsons MR, Phillips SEV, Knowles PF, McPherson MJ. Conserved tyrosine-369 in the active site of *Escherichia coli* copper amine oxidase is not essential. Biochemistry. 2001; 40:12808–12818. [PubMed: 11669617]

14. McPherson, A. Crystallization of Biological Macromolecules. Cold Spring Harbor Laboratory Press; Cold Spring Harbor, New York: 1999.

15. Otwinowski Z, Minor W. Processing of X-ray diffraction data collected in oscillation mode. Methods Enzymol. 1997; 276:307–326.

16. Navaza J. AMoRe: an automated package for molecular replacement. Acta Cryst. A. 1994; 50:157–163.

17. CCP4. Collaborative Computational Project, Number 4. The CCP4 suite: programs for protein crystallography. Acta Crystallogr. Sect. D Biol. Crystallogr. 1994; 50:760–763. [PubMed: 15299374]

18. Brünger AT, Adams PD, Clore GM, DeLano WL, Gros P, Grosse-Kunstleve RW, Jiang J, Kuszewski J, Nilges M, Pannu NS, Read RJ, Rice LM, Simonson T, Warren GL. Crystallography & NMR system: a new software suite for macromolecular structure determination. Acta Cryst. D. 1996; 54:905–921.

19. Cai DY, Klinman JP. Copper amine oxidase: heterologous expression, purification and characterization of an active enzyme in *Saccharomyces cerevisiae*. Biochemistry. 1994; 33:7647–7653. [PubMed: 8011631]

20. Cai DY, Williams NK, Klinman JP. Effect of metal on 2,4,5-trihydroxyphenylalanine (topa) quinone biogenesis in the *Hansenula polymorpha* copper amine oxidase. J. Biol. Chem. 1997; 272:19277–19281. [PubMed: 9235922]

21. Laskowski R, Thornton J, Moss D, MacArthur M. *PROCHECK*: a program to check the stereochemical quality of protein structures. J. Appl. Cryst. 1993; 26:283–291.

22. Kraut DA, Sigala PA, Fenn TD, Herschlag D. Dissecting the paradoxical effects of hydrogen bond mutations in the ketosteroid isomerase oxyanion hole. Proc. Natl. Acad. Sci. USA. 2010; 107:1960–1965. [PubMed: 20080683]

23. Schwartz B, Green EL, Sanders-Loehr J, Klinman JP. Relationship between conserved consensus site residues and the productive conformation for the TPQ cofactor in a copper-containing amine oxidase from yeast. Biochemistry. 1998; 37:16591–16600. [PubMed: 9843426]

24. Dove JE, Schwartz B, Williams NK, Klinman JP. Investigation of spectroscopic intermediates during copper-binding and TPQ formation in wild-type and active site mutants of a copper-containing amine oxidase from yeast. Biochemistry. 2000; 39:3690–3698. [PubMed: 10736168]

25. Kim M, Okajima T, Kishishita S, Yoshimura M, Kawamori A, Tanizawa K, Yamaguchi H. X-ray snapshots of quinone cofactor biogenesis in bacterial copper amine oxidase. Nature Struct. Biol. 2002; 9:591–596. [PubMed: 12134140]

NIH-PA Author Manuscript

NIH-PA Author Manuscript

NIH-PA Author Manuscript

26. Chen Z-W, Schwartz B, Williams NK, Li RB, Klinman JP, Mathews FS. Crystal structure at 2.4Å resolution of zinc-substituted copper amine oxidase of *Hansenula polymorpha* expressed in *E. coli*. Biochemistry. 2000; 39:9709–9717. [PubMed: 10933787]

27. Kleywegt GJ, Brünger AT. Chemking your imagination: application of the free r value. Structure. 1996; 4:897–904. [PubMed: 8805582]

NIH-PA Author Manuscript

NIH-PA Author Manuscript

NIH-PA Author Manuscript

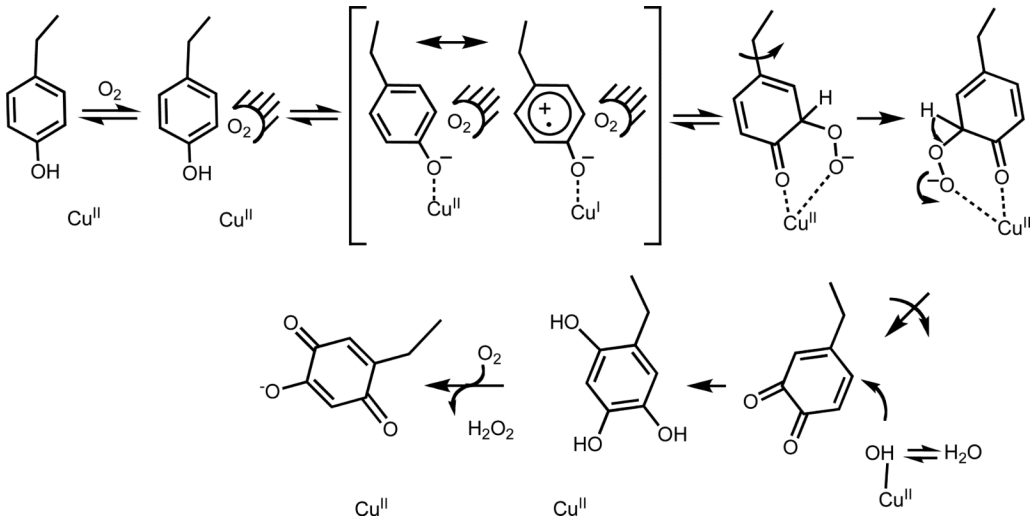

Scheme 1.
Proposed mechanism for the biogenesis of TPQ.

NIH-PA Author Manuscript

NIH-PA Author Manuscript

NIH-PA Author Manuscript

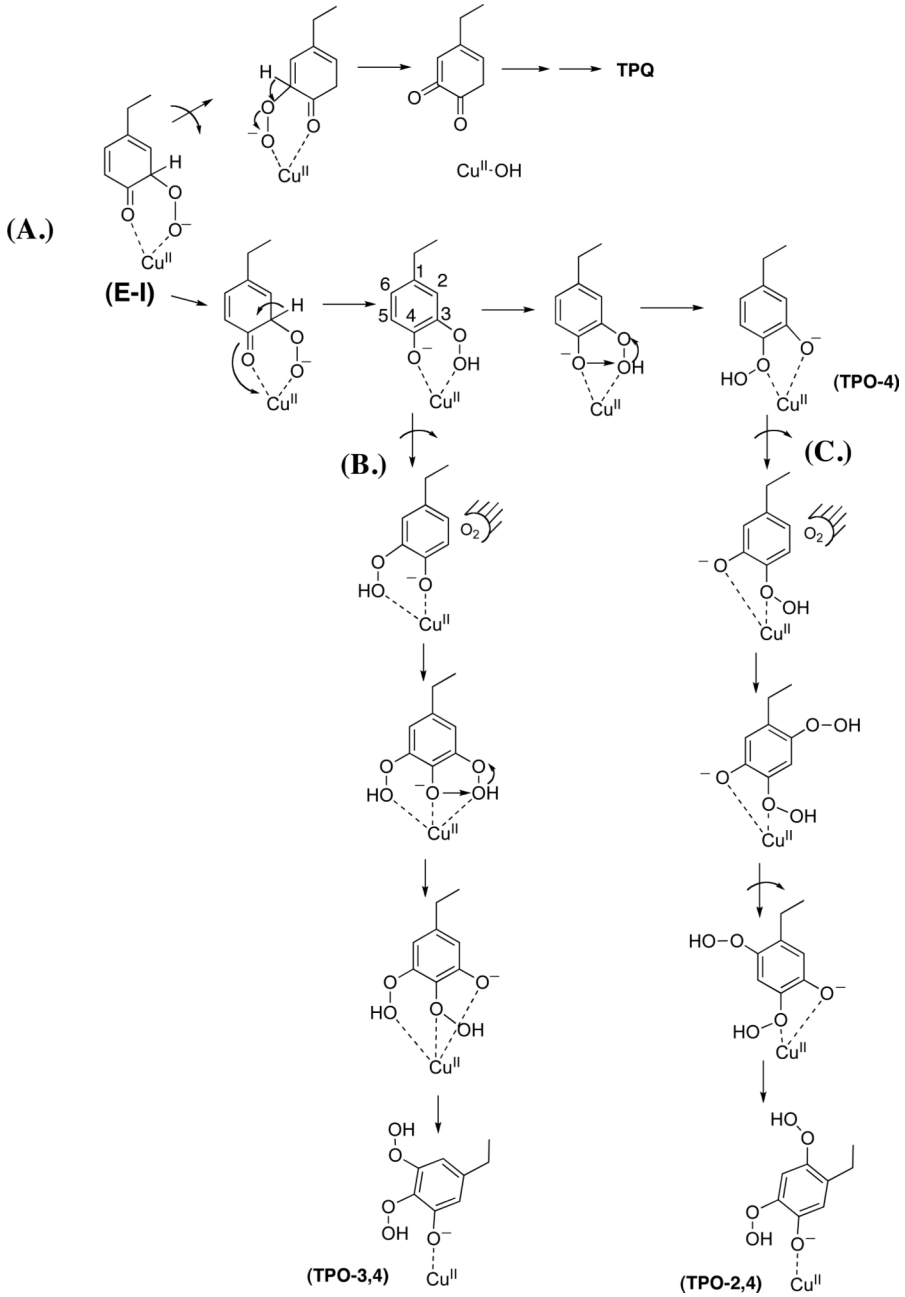

Scheme 2.

A. Mechanism for the branching of a biogenesis intermediate to TPQ and TPO. **B**. Model to explain partial occupancy of a derivative at C-3 via formation of TPO-3,4. **C**. Model to explain partial occupancy of a derivative at C-2 via formation of TPO-2,4.

NIH-PA Author Manuscript

NIH-PA Author Manuscript

NIH-PA Author Manuscript

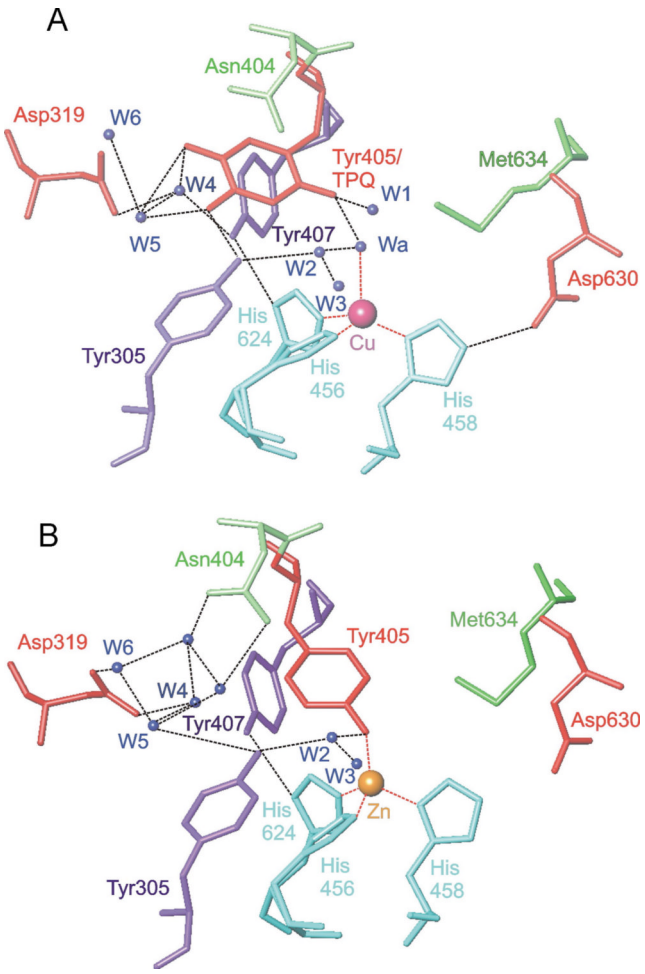

Figure 1.

A. Mature HPAO active site, with TPQ in the reactive conformation (6). Acidic side chains are red, basic are cyan, aromatic are purple, neutral hydrophilic are lime and hydrophobic are green, the TPQ is red and the Cu(II) ion is crimson. A network of 6 active-site water molecules (W1-W6) and one axial copper-coordinating water (Wa) that forms hydrogen bonds to TTQ and side chain atoms (6) are shown in blue. A 7th water, We, is also coordinated to the Cu(II) ion but is not shown. Hydrogen and metal coordination bonds are shown as black and red dashed lines, respectively. **B.** Precursor HPAO active-site (21), Zn(II) (gold) and unmodified Tyr405 (red). The color schemes for atoms and coordination or hydrogen bonds are as in **Figure 1A** (These figures are reprinted from (8)).

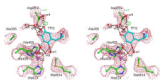

Figure 2.
A stereo view of the Y305A mutant of HPAO. The (2Fo-Fc) electron density map (red contours at the 1σ level, dark blue at the 8 σ level) and the (Fo–Fc) electron density (green contours at the +3σ level) are shown (no contours are present at the -3 σ level). Also shown is the 6-fold averaged simulated annealing (Fo–Fc) omit map (cyan contours at the +3 σ level). Carbon atoms are green except for TPQ where carbon atoms are cyan; nitrogen atoms are blue, oxygen red, sulfur yellow, and copper magenta. Hydrogen bonds are shown as dashed black lines and coordination bonds as dashed crimson lines. All of the active-site water molecules present in the wild-type structure are shown (wa, w1-w6, shown in Figure 1A, plus an additional water, w7) are shown. Water we, present in the wild-type structure, is not visible in the Y305A mutant.

NIH-PA Author Manuscript
NIH-PA Author Manuscript
NIH-PA Author Manuscript

NIH-PA Author Manuscript

NIH-PA Author Manuscript

NIH-PA Author Manuscript

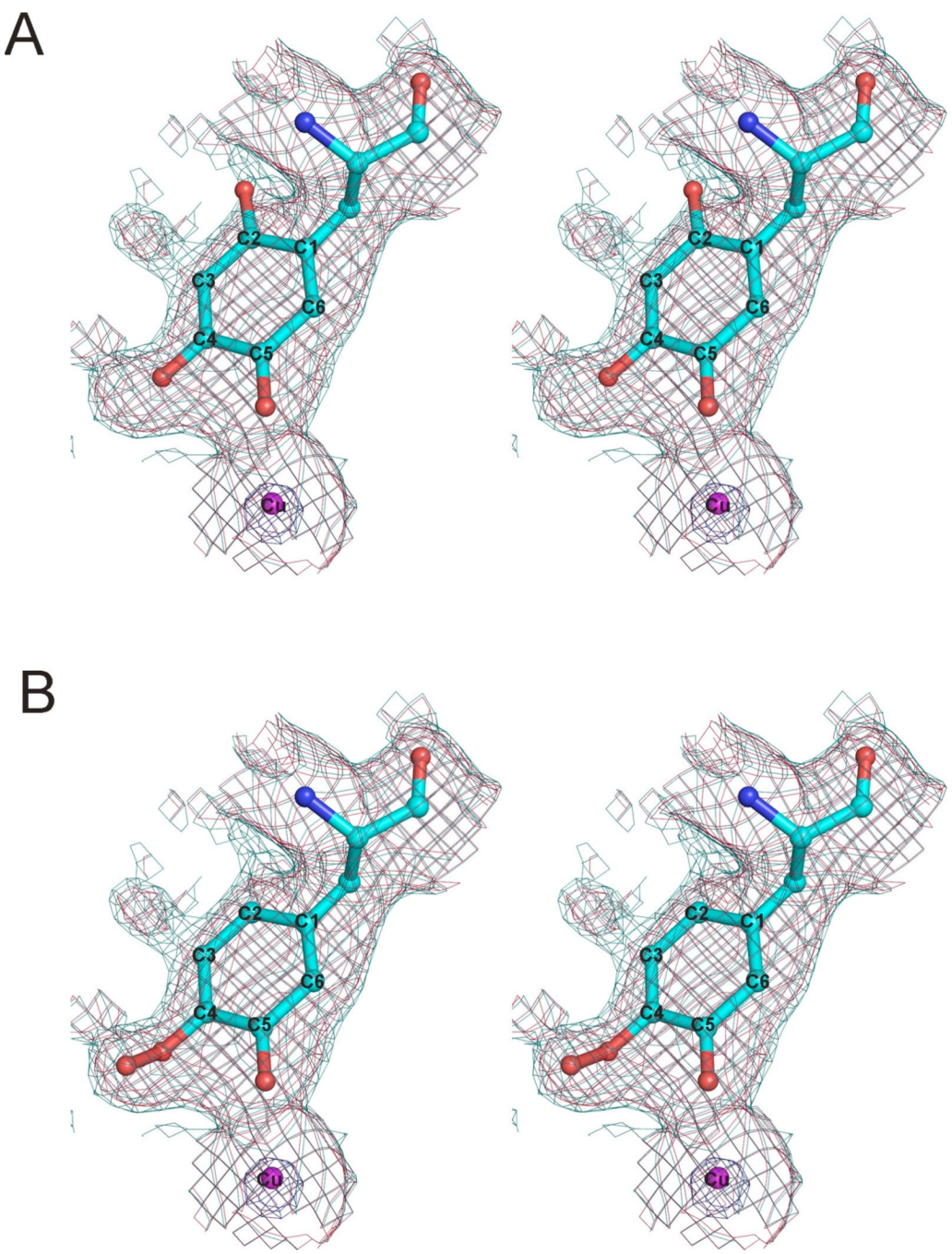

NIH-PA Author Manuscript

NIH-PA Author Manuscript

NIH-PA Author Manuscript

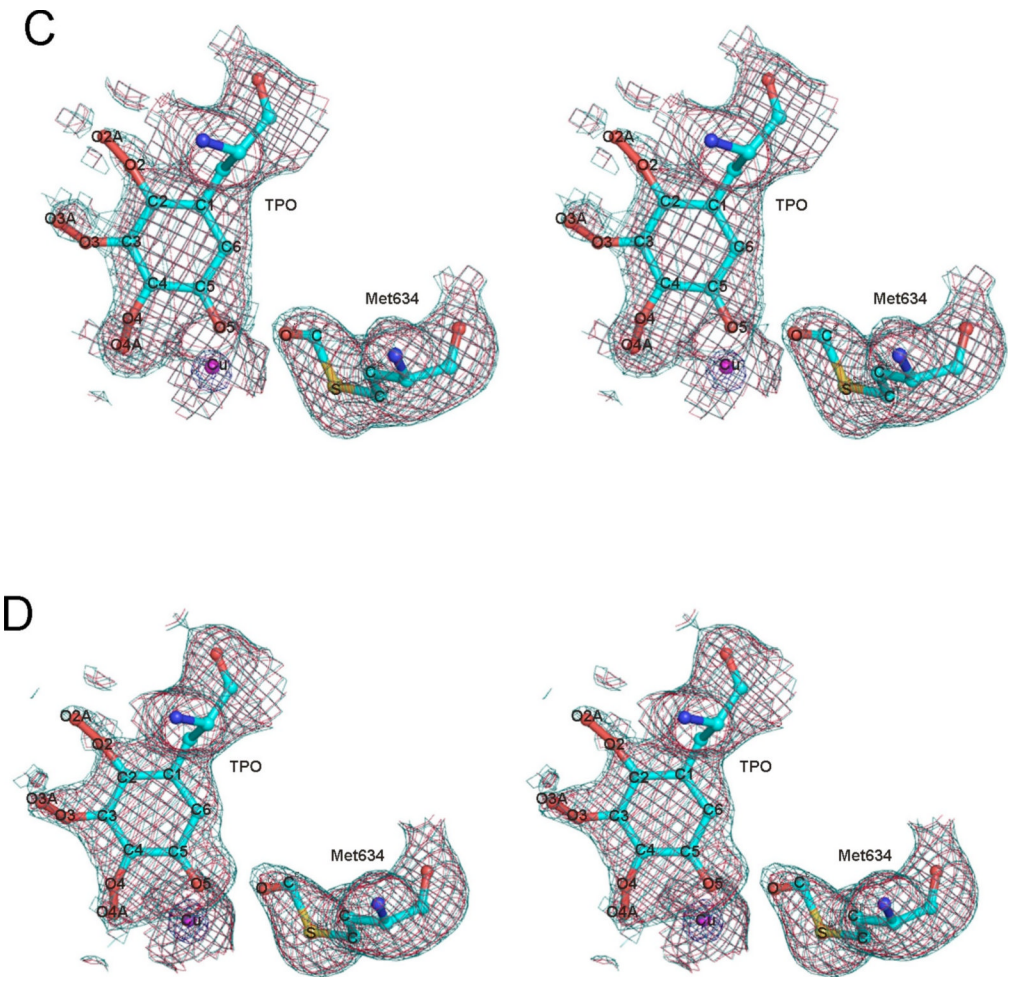

Figure 3.

Simulated annealing omit maps of the Y305F mutants of HPAO computed using coefficients (Fo–Fc) where Fc were calculated from models in which the side chain of residue 405 was absent; in panels A-C Fo were the structure factors observed from crystals of the *E-coli*-expressed mutant and in panel D from the yeast-expressed mutant. The maps are contoured at sigma levels of 2.5 (cyan), 3.0 (crimson) and 10.0 (purple). Atoms are colored blue for nitrogen, red for oxygen, and magenta for copper; for the residue 405 cofactor, the carbon atoms are cyan. **A**. Stereo view of a model of TPQ is shown superimposed on the omit map. **B**. Stereo view of an initial model of TPO is superimposed on the map. **C** and **D**. Stereo views of the final model of TPO superimposed on the *E. coli*- and yeast-expressed simulated annealing omit maps, respectively, of the Y305F mutants. In addition, the modified methionine at position 634 (also omitted during the omit map calculation) is shown superimposed on its density.

NIH-PA Author Manuscript

NIH-PA Author Manuscript

NIH-PA Author Manuscript

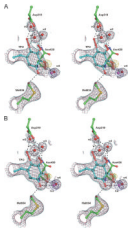

Figure 4.

Final electron density maps of the Y305F mutants of HPAO computed using coefficients (2Fo–Fc) and (Fo–Fc) where Fc was calculated from the models refined with TPO and the modified Met634 present. The (2Fo–Fc) maps are contoured at the 0.8 (cyan), 1.0 (crimson) and 8.0 (dark blue) σ levels and the (Fo–Fc) maps are contoured at the -3.0 σ level (gold); no contours above the +3.0 σ level are present. Contours are drawn for the TPO and modified Met634 side chains, as well as for waters, w1-w4. The side chains of Asp319 and Asn430 are also shown without contours (for clarity). Hydrogen and coordination bonds are indicated by black dashed lines. The atom coloring and numbering scheme is the same as in Figure 3 with the additional numbering of four water molecules, w1-w4. These four waters correspond closely to the active site waters found in the native and Y305A structures, namely, waters w4, w7, w5 and w3, respectively. The residues, waters and cofactor oxygen atoms are labeled. **A**. The *E. coli*-expressed structure is shown. **B**. The yeast-expressed structure is shown.

NIH-PA Author Manuscript

NIH-PA Author Manuscript

NIH-PA Author Manuscript

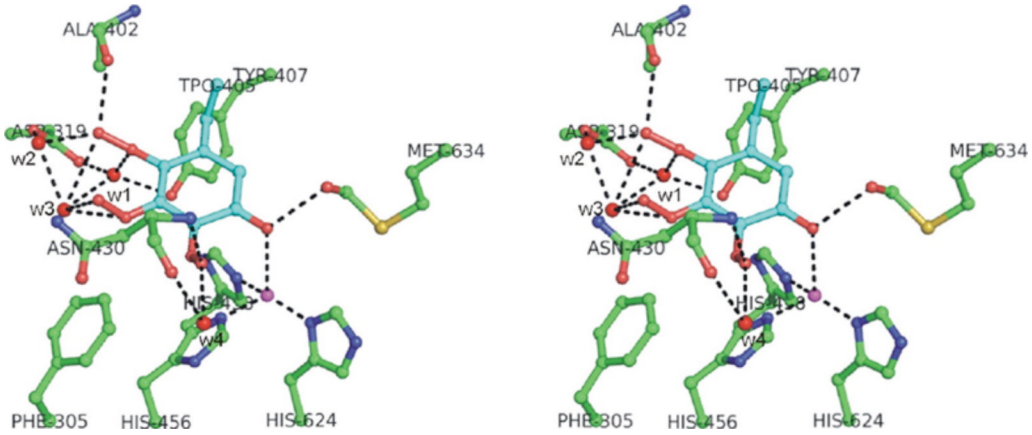

Figure 5.

Active-site configuration for the final model of the *E. coli*-expressed Y305F mutant of HPAO. The orientation of the molecule is approximately the same as shown in Figure 1A. The final TPO cofactor and modified Met634 side chain are shown along with four water molecules, w1-w4. Also included are the side chains of His456, His458, and His624 that form three of the four coordination bonds to copper. In addition, shown are the side chains of Phe305, Asp319, Ala402, and Asn430. Hydrogen and coordination bonds are indicated by black dashed lines. The atom coloring scheme is the same as described for Figure 3.

NIH-PA Author Manuscript

NIH-PA Author Manuscript

NIH-PA Author Manuscript

Table 1

Compilation of kinetic parameters for Y305A and Y305F during catalysis and TPQ biogenesis.

Parameter	WT	Y305F	Y305A	Y305F/Y305A
k_{cat}, s^{-1} *a*	20	0.16	7.5	0.021
k_{bio}, min^{-1} *b*	0.08	0.024	0.0025	9.6

a For oxidation of ethylamine at pH 7. From Ref (7).

b For biogenesis at pH 7. From Ref (8).

NIH-PA Author Manuscript
NIH-PA Author Manuscript
NIH-PA Author Manuscript

Table 2

Data collection and refinement statistics.

Mutant	**Y305A Yeast**	**Y305F Yeast**	**Y305F E. Coli**
Expression system	*S. cerevisiae*	*S. cerevisiae*	*E. coli*
Space group	$P2_12_12_1$	$P2_1$	$P2_1$
Cell constants (a, b, c: Å, β)	138.91, 147.15, 233.76.90°	96.29, 232.47, 104.31, 93.68°	94.52, 232.62, 104.15, 91.51°
Number of observations	476664	933972	692670
Number of unique reflections	134330	313044	217301
Average multiplicity	3.5	3.0	3.2
Resolution limits (outer shell)	30-2.5Å (2.6-2.5Å)	100-1.90 (1.97-1.90)	100-2.05Å (2.12-2.05Å)
R_{merge}[a] (%)	7.2 (22.4)	6.0 (46.3)	6.7 (31.8)
Completeness (%)	79.1 (41.0)	87.4 (53.9)	77.4 (51.9)
$<I/\sigma(I)>$[b]	14.1 (3.1)	17.2 (2.2)	14.2 (3.3)
Resolution range for refinement (Å)	30-2.5	6.0-1.9	40-2.05
Reflections used for refinement	134165	272421	205462
Working set	120767	258930	195210
Test set	13398	13491	10252
R_{cryst}[c] (%)	18.5	21.3	19.3
R_{free}[d] (%)	19.8	21.7	20.0
Number of non-hydrogen protein atoms[e]	5187	5198	5235
Number of solvent molecules	517	456	506
Number of copper ions[e]	1	1	1
Number of phosphate Ions	0	3	0
Extent of protomer Resolved	Pro18-Val672	Pro18-Val672	Ala15-Glu675
RMSD bond lengths (Å)	0.010	0.006	0.006
RMSD bong angles (°)	1.7	1.6	1.6
Mean B factor (Å^2)			
Protein	28.9	27.0	28.5
Solvent	35.4	31.8	37.0
Copper ion	31.2	23.1	26.2
RMS ΔB (main chain-main chain)	1.1	1.5	1.3
RMS ΔB (main chain-side chain	1.4	1.8	1.7
RMS ΔB (side chain-side chain)	2.1	3.2	2.9
Ramachandran plot (%)			
Allowed region	99.4	99.6	99.3
Generously allowed region	0.4	0.2	0.5
Disallowed region	0.2	0.2	0.3

[a] $R_{merge}=\Sigma_h\Sigma_i I(h)-I_i(h)/\Sigma_h\Sigma_i I_i(h)$, where $I_i(h)$ and I(h) are the ith and mean measurements of reflection h.

NIH-PA Author Manuscript

NIH-PA Author Manuscript

NIH-PA Author Manuscript

[b] $I/\sigma(I)$ is the average signal to noise ratio for merged reflection intensities.

[c] $R=\Sigma_h Fo-Fc/\Sigma_h Fo$, where Fo and Fc are the observed and calculated structure factor amplitudes of reflection h.

[d] R_{free} is the test reflection data set, about 5-10 % selected randomly for cross validation during crystallographic refinement (Ref. 27).

[e] Number of atoms in one independent protomer refined using strict NCS.